All fiber-coupled, long-term stable timing distribution for free-electron lasers with few-femtosecond jitter

K. Şafak, M. Xin, P. T. Callahan, M. Y. Peng, and F. X. Kärtner


Articles you may be interested in

A beam branching method for timing and spectral characterization of hard X-ray free-electron lasers
Struct. Dyn. **3**, 034301 (2016); 10.1063/1.4939655

Generating femtosecond X-ray pulses using an emittance-spoiling foil in free-electron lasers
Appl. Phys. Lett. **107**, 191104 (2015); 10.1063/1.4935429

Response-time improved hydrothermal-method-grown ZnO scintillator for soft x-ray free-electron laser timing-observation
Rev. Sci. Instrum. **81**, 033102 (2010); 10.1063/1.3310276

Efficiency enhancement of a two-beam free-electron laser
Phys. Plasmas **16**, 123105 (2009); 10.1063/1.3272094

Femtosecond synchronism of x rays to visible light in an x-ray free-electron laser
Rev. Sci. Instrum. **76**, 063304 (2005); 10.1063/1.1927109
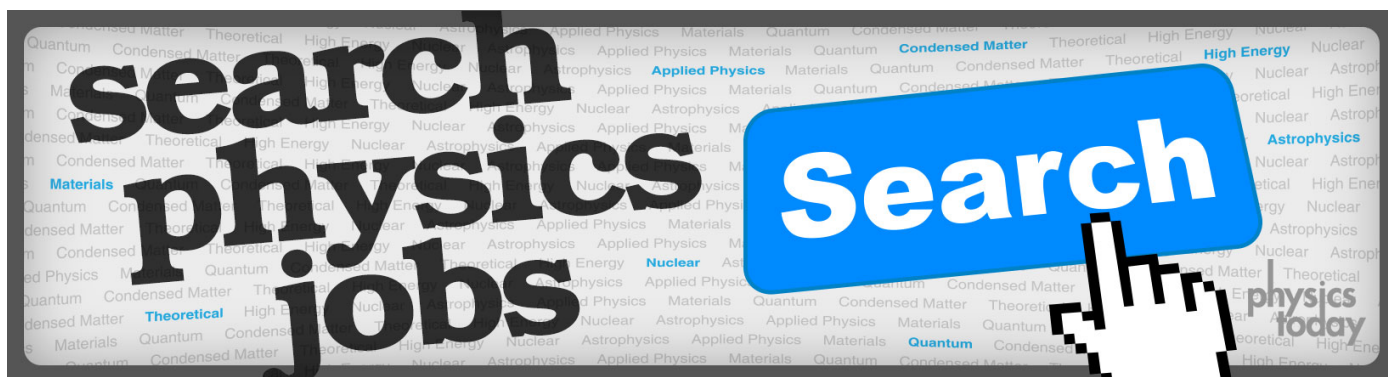
All fiber-coupled, long-term stable timing distribution for free-electron lasers with few-femtosecond jitter

K. Şafak,[1,2,a)] M. Xin,[1] P. T. Callahan,[3] M. Y. Peng,[3] and F. X. Kärtner[1,2,3]

[1]*Center for Free-Electron Laser Science, Deutsches Elektronen-Synchrotron, Notkestrasse 85, Hamburg 22607, Germany*
[2]*Physics Department, University of Hamburg and the Hamburg Center for Ultrafast Imaging, Luruper Chaussee 149, Hamburg 22761, Germany*
[3]*Department of Electrical Engineering and Computer Science and Research Laboratory of Electronics, Massachusetts Institute of Technology, Cambridge, Massachusetts 02139, USA*

We report recent progress made in a complete fiber-optic, high-precision, long-term stable timing distribution system for synchronization of next generation X-ray free-electron lasers. Timing jitter characterization of the master laser shows less than 170-as RMS integrated jitter for frequencies above 10 kHz, limited by the detection noise floor. Timing stabilization of a 3.5-km polarization-maintaining fiber link is successfully achieved with an RMS drift of 3.3 fs over 200 h of operation using all fiber-coupled elements. This all fiber-optic implementation will greatly reduce the complexity of optical alignment in timing distribution systems and improve the overall mechanical and timing stability of the system. © 2015 Author(s). All article content, except where otherwise noted, is licensed under a Creative Commons Attribution 3.0 Unported License.
[http://dx.doi.org/10.1063/1.4922747]

I. INTRODUCTION

New generation free-electron lasers (FELs) are presently the only facilities which can generate coherent light pulses with unprecedented brightness and spatial resolution in the hard X-ray regime.[1–4] Recent developments in X-ray pulse characterization have shown that conventional FELs operating with self-amplified spontaneous emission can produce X-ray pulses with temporal durations well below 100 fs and up to 10^{13} photons per pulse.[5] The combination of unprecedented brightness with angstrom-level spatial- and femtosecond-level temporal-resolution opens up many new possibilities for time-resolved pump-probe experiments.[6,7] High precision timing distribution systems are critical for FELs for two primary reasons. First, the temporal duration of the X-ray pulses is determined by the final compression of the electron bunch, which is highly sensitive to the overall synchronization between the photo-injector laser, the linear accelerators, and the bunch compressors. Progressively shorter X-ray pulses will require more precise timing distribution between these components. Second, tight synchronization between the FEL pulses and external lasers is needed for pump-probe experiments aiming high temporal resolution. Next generation FELs, such as Linac Coherent Light Source II in Stanford and the European X-ray FEL (XFEL) in Hamburg, are predicted to deliver X-ray pulses even shorter than 10 fs.[8] Unlocking the high temporal-resolution capabilities of these facilities will require extremely stable timing distribution systems delivering better than 10-fs precision between optical and radio frequency (RF) sources located over kilometer distances. Traditional RF-signal distribution approach which depend solely on photodetection and electronic phase-locking techniques cannot deliver better than ∼100-fs RMS jitter across the facility, thus preventing FELs from operating at their full potential.[9–11]

a)Author to whom correspondence should be addressed. Electronic mail: kemal.shafak@desy.de

Over the past decade, we have been advancing a pulsed-optical timing distribution system that uses the ultralow-noise pulse train from a mode-locked laser as its timing signal.[12] Since a mode-locked laser can simultaneously generate ultralow-noise optical and microwave signals in the form of optical pulse trains,[13,14] it has the inherent advantage of enabling high-precision time signals that can be distributed to synchronize multiple microwave and optical sources at different locations. As depicted in Fig. 1(a), the timing signal of the master laser is transferred through timing-stabilized fiber links using balanced optical cross–correlators (BOC)[15] from a central location to multiple end stations, where efficient and robust synchronization is realized again with BOCs for optical sources[16] and balanced optical-microwave phase detectors for RF sub-systems.[17,18] Timing detection principle of a BOC is shown in Fig. 1(b). Two pulses whose relative jitter to be measured are launched into a nonlinear crystal in a double-pass configuration. As they propagate through the crystal, they walk through each other due to the difference in their group velocities and generate different amounts of sum-frequency (SF) light depending on their temporal overlap in forward and reverse pass. The generated SF pulses are separated from the fundamental harmonics by dichroic beam splitters at the end of each pass and measured by two separate photodetectors of a balanced receiver. The difference in detected SF power gives a voltage signal only proportional to the time separation of the pulses by suppressing effects of optical intensity fluctuations.[16] BOC is suitable for optical pulses with either the same or different center wavelengths. For the former case, one has to choose a nonlinear crystal with type-II phase matching and introduce group delays using birefringence. This scheme is also used here to measure propagation time fluctuations of the timing signals upon transmission in the fiber links and then compensate for them by applying feedback to a variable delay element.

Recent experimental results performed in test-beds under laboratory conditions indicate that this approach is capable of delivering sub-fs precision stabilization of multi-km long fiber links and remote laser synchronization using free-space optics and BOCs.[19–21] Such a pulsed-optical timing distribution has been already implemented at the Free-electron Laser in Hamburg (FLASH) and achieved facility-wide timing better than 30 fs RMS for 90-fs X-ray pulses.[22]
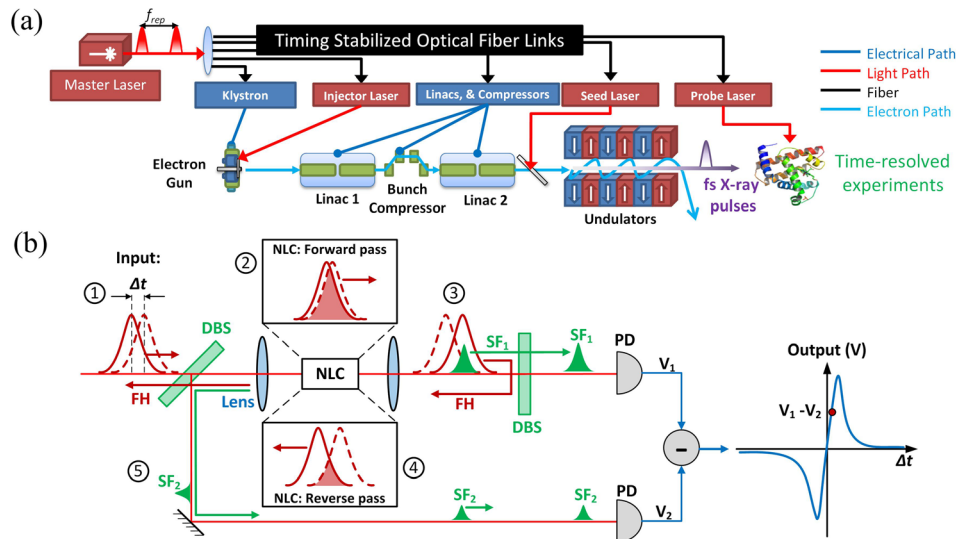

FIG. 1. (a) Pulsed-optical synchronization scheme for an FEL facility. A low-noise mode-locked laser serves as the reference clock and provides all independent components of the FEL with optical synchronization signals through timing stabilized fiber links using BOCs. (b) An illustration of the BOC timing detection scheme. Two input pulses (represented with red solid and dashed lines) propagate through the nonlinear crystal at different speeds and generate different amounts of light at their sum-frequency (represented as green pulses) on the forward and reverse pass. The difference in detected sum-frequency power gives an output voltage signal proportional to the initial time separation between the pulses Δt. Abbreviations: FH: input pulses at fundamental harmonics; DBS: dichroic beam splitter; NLC: nonlinear crystal; SF_1 and SF_2: generated sum-frequency light on the forward and reverse pass, respectively; PD: photodetector; and V_1 and V_2: photodetected voltages for SF_1 and SF_2.

Real facilities like FLASH or the European XFEL need fiber networks consisting of 10 or more timing links, which require tremendous attention to the alignment and stability of the free-space optics to minimize timing-drifts induced by beam pointing instabilities.[23] This situation also necessitates preamplification of the master laser's output to overcome excessive free-space to fiber coupling losses to provide adequate power for all timing links. To eliminate free-space optics and its disadvantages from the timing distribution system, we have developed integrated, fiber-coupled BOC (FC-BOC) using periodically poled $KTiOPO_4$ (PPKTP) waveguides.[24,25] These waveguides exhibit second harmonic (SH) conversion efficiencies up to $\eta_0 = 1.02\%/$ [W·cm^2] (20 times higher than the bulk optical devices), which will decrease the power demand from the master laser and consequently support more timing links. Furthermore, the robustness and ease of implementation of these fiber-coupled devices will eliminate alignment-related problems observed in free-space optics. In this work, we present an all-fiber implementation of the pulsed-optical timing distribution system using FC-BOCs. This paper starts with the timing jitter characterization of the master laser and then details the timing link stabilization experiment using all fiber-coupled elements.

II. TIMING JITTER CHARACTERIZATION OF THE MASTER LASER

A. Experimental setup

Low-noise performance of the master laser is of tremendous importance and precise noise characterization measurements are necessary to choose the laser with the lowest possible jitter. We characterized the jitter performance of the master laser using the BOC method as illustrated in Fig. 2.[26] The cross-correlator used here is based on polarization-dependent type-II SH generation in a PPKTP crystal and requires two identical mode-locked lasers whose repetition rates are locked to each other. The master laser is an Origami-15 from Onefive GmbH operating at 1554-nm center wavelength with +22.4-dBm average output power, 150-fs pulse width, and 216.66-MHz repetition rate. The slave laser is another Origami-15 with a central wavelength at 1553 nm, a repetition rate of 216.67 MHz with an output power of +22.1 dBm and a pulse duration of 172 fs.

Starting with these two lasers, we combine the output pulse streams with orthogonal polarizations in a BOC. The error signal is fed back to the piezoelectric transducer (PZT) of the slave laser, in order to lock its repetition rate to that of the master laser. Electrical power spectral density of the BOC output when observed with a baseband spectrum analyzer is converted to jitter spectral density by using the sensitivity of the BOC (0.36 mV/fs measured with a balanced photodetector (BPD) of 2×10^3 V/A transimpedance gain and 1-MHz bandwidth). Once locked, the lasers' inherent jitter can be observed directly for frequencies beyond the locking bandwidth. Since these two lasers are almost identical, the measured spectral power density is divided by two to find the jitter contribution of one laser. From a simple feedback-loop analysis, the locking bandwidth of the BOC can be calculated as[21]
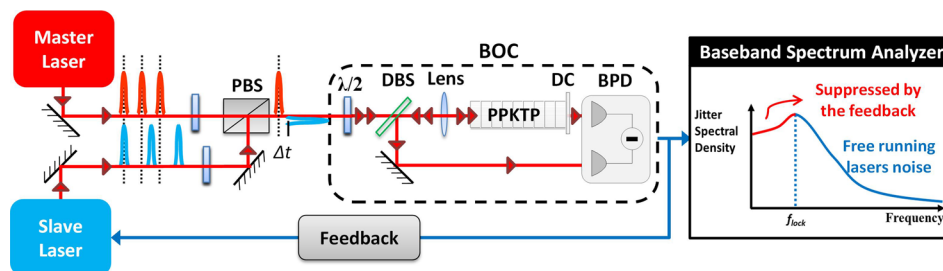

FIG. 2. Experimental setup for timing jitter characterization using a BOC. Abbreviations: $\lambda/2$: half-wave plate; PBS: polarization beam splitter; Δt: timing mismatch between two pulse streams; DBS: dichroic beam splitter; PPKTP: periodically poled potassium titanyl phosphate crystal; DC: dichroic coating; and BPD: balanced photodetector.

$$f_{lock} = \sqrt{\frac{K}{2}\left[K - 2f_{PI} + \sqrt{(K - 2f_{PI})^2 + 4f_{PI}^2}\right]}, \tag{1}$$

where $K = K_{BOC}K_{PI}K_{PZT}/(2\pi f_{rep})$ and K_{BOC} (V/fs) and K_{PZT} (Hz/V) are the sensitivities of the BOC and of the slave laser's PZT, respectively. f_{PI} and K_{PI} are the corner frequency and the gain of the proportional-integral (PI) servo controller, and f_{rep} is the repetition rate of the master laser. By using some typical values observed in our experiment: $K_{\text{BOC}} = 0.36\,\text{mV/fs}$, $K_{PZT} = 10\,\text{Hz/V}$, $f_{rep} = 216.66\,\text{MHz}$, $K_{PI} = 10$, and $f_{PI} = 3\,\text{kHz}$, f_{lock} can be calculated to be approximately 23 kHz. With these feedback parameters, the observed range of the laser's inherent jitter will be the frequencies above 23 kHz, since the feedback loop will suppress the noise spectrum below the locking bandwidth.

B. Results and discussion

Fig. 3(a) shows the jitter spectral density of the master laser from 10 Hz up to 1 MHz for varying servo controller gain settings. As can be inferred from Eq. (1), a high servo gain value would lead to a large locking bandwidth, which in turn would not allow the inherent jitter of the laser to be observed for low frequencies. Therefore, the measured jitter spectral densities with gain values above 10 dB in Fig. 3(a) correlate only with the other spectra for frequencies higher than 10 kHz. As the servo gain is decreased, the locking bandwidth is reduced and the inherent jitter of the laser is revealed for offset frequencies below 1 kHz (see the spectra for 0 dB gain or lower in Fig. 3(a)). Due to the low timing jitter of the laser, the jitter spectral density above 30 kHz is obscured by the noise floor of the measurement (dashed black curve in Figs. 3(a) and 3(b)). The measurement result shown in Fig. 3(b) corresponds to the timing jitter spectral density between 1 kHz and 1 MHz taken for −10 dB servo gain. The integration of the
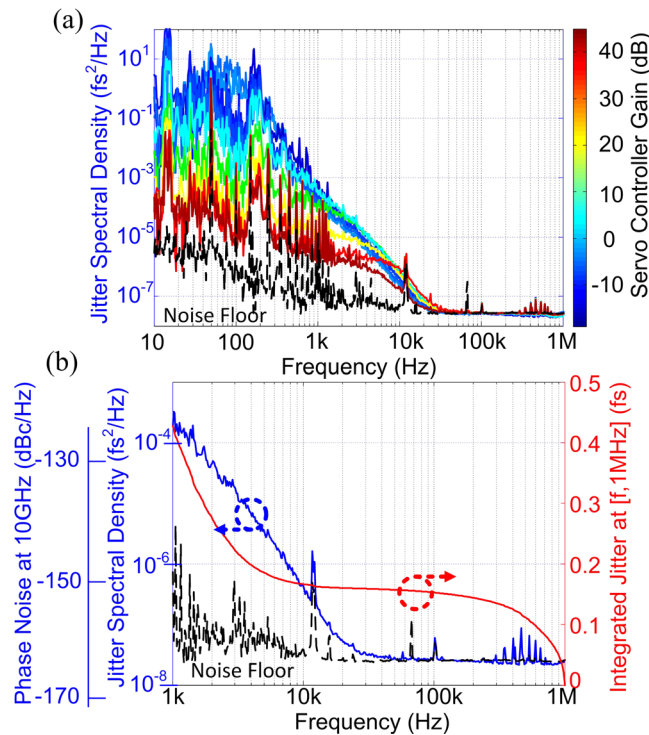

FIG. 3. (a) Timing jitter spectral density of the master laser for varying servo controller gain. The color code indicates the servo controller gain values of the individual spectra. (b) Blue curve: jitter spectrum and single-sideband phase noise (scaled at a 10 GHz carrier) for −10 dB servo gain; red curve: integrated timing jitter. The noise floor is determined by measuring the output of the balanced detector when the input is blocked and plotted as dashed-black lines on both graphs.

spectrum results in an extremely low jitter of approximately 400 attoseconds (as), for frequencies between 1 kHz and 1 MHz. Due to the fact that operational locking bandwidths for our applications are expected to be higher than 10 kHz, the relevant frequency range for the integrated jitter is between 10 kHz and 1 MHz. In this range, the master laser exhibits an integrated jitter of 170 as. Although, the true value will be even lower since the laser jitter above 30 kHz is limited by the detection noise floor. Thus, this laser is well suited for the development of a precise timing distribution system.

III. ALL FIBER-COUPLED TIMING DISTRIBUTION THROUGH A 3.5-km FIBER LINK

Fiber-optic links are the preeminent choice to efficiently deliver optical signals to remote locations. However, in an unstabilized link, environmental fluctuations (such as temperature, humidity, and mechanical stress) will induce errors in the arrival time of the delivered optical pulses. Hence, one has to ensure drift- and jitter-free distribution of the pulsed-signal from the master laser in order to construct a high precision timing distribution system. Here for the first time, we show an all fiber-optic implementation of a timing link stabilization with FC-BOCs delivering 3.3-fs RMS precision over 200 h of continuous operation.

A. Experimental setup

A diagram of the experimental setup is shown in Fig. 4(a). The master laser is an Origami-15 with the output parameters as discussed in Sec. II. Its repetition rate is locked to a RF synthesizer to reduce the timing drift for frequencies below 10 Hz. The only free-space part built in this experiment is the initial power separation elements comprised of one polarization beam splitter (PBS) and 3 half-wave plates. Furthermore, polarization-maintaining (PM) fiber components are chosen over standard single-mode (SM) fiber for the construction of the setup, as previous results obtained with SM fiber have showed substantial polarization-mode-dispersion effects in the out-of-loop link stabilization measurements.[27] After the PBS, the output of the master laser is coupled into two separate fiber paths: the out-of-loop reference path and the link stabilization unit. The out-of-loop reference path is a 1-m long PM fiber serving as the reference arm for the out-of-loop FC-BOC. The link stabilization unit starts with a FC-PBS1
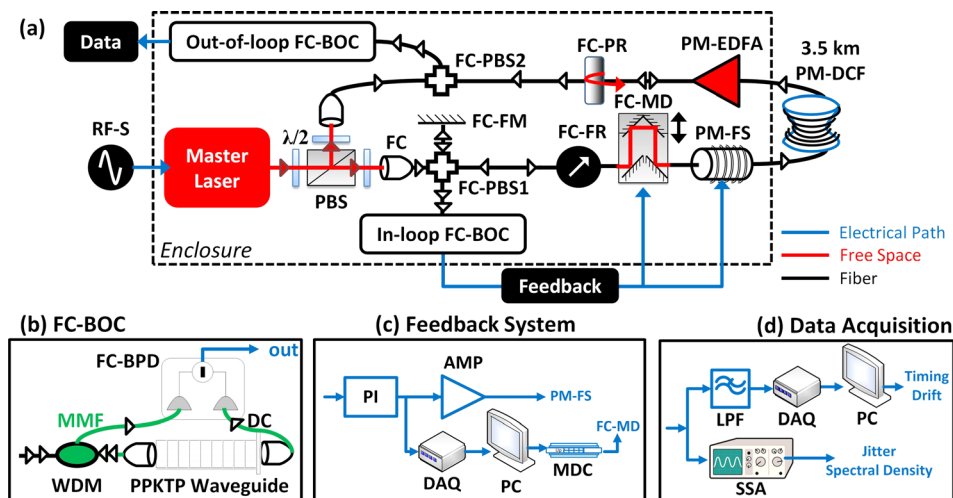

FIG. 4. (a) Schematic of the link stabilization experiment. (b) Main elements are the FC-BOCs. (c) Feedback system employed for the link delay compensation. (d) Data acquisition elements for the evaluation of the out-of-loop measurement results. Abbreviations: RF-S: RF synthesizer; FC: fiber coupler; FC-PBS: FC polarization beam splitter; FC-FM: FC Faraday mirror; FC-FR: FC Faraday rotator; FC-MD: FC motorized delay; PM-FS: PM fiber stretcher; PM-DCF: PM dispersion-compensated fiber; PM-EDFA: PM erbium doped fiber amplifier; FC-PR: fiber-coupled partial reflector; WDM: wavelength division multiplexer; MMF: multi-mode fiber; DC: dichroic coating; FC-BPD: fiber-coupled BPD; PI: proportional-integral controller; AMP: voltage amplifier; DAQ: data acquisition card with 1-Hz sampling rate; PC: personal computer; MDC: motorized delay controller; LPF: 2-Hz low-pass filter; and SSA: Agilent 5052a signal source analyzer.

which divides the optical power further into two segments. The first segment (traveling to the right through FC-PBS1 in Fig. 4(a)) is directed into the timing link which consists of a FC Faraday rotator (FC-FR), a FC motorized delay line (FC-MD) with 560-ps range, a PM fiber stretcher (PM-FS), and a 3.5-km PM dispersion-compensated fiber spool (PM-DCF). The second segment is sent into a 0.5-m fiber having a FC Faraday mirror (FC-FM) at the end. The FC-FM turns the polarization of the pulses by $\pi/2$ upon reflection and guides them into the in-loop FC-BOC to serve as the reference pulses for the timing stabilization of the 3.5-km link.

Both of the FC-BOCs used in this experiment are PPKTP waveguide chips in fiber-coupled packages with internal temperature control.[25] A schematic of the module is shown in Fig. 4(b). The wavelength division multiplexer (WDM) consists of a fiber-coupled dichroic beam-splitter cube coupling the input pulses into the waveguide for cross-correlation and separates the SH return path from the fundamentals. The forward and backward SH signals are then fed to the ports of a BPD.

Power management of the fiber links is critical: high link output power is desirable for high signal-to-noise ratio, while low link operating power is needed to avoid fiber nonlinearity-induced timing errors. As a precaution, the fibers are operated with a maximum power of $+13$ dBm to avoid significant fiber nonlinearities. The input power to the timing link is set to $+8$ dBm such that after forward propagation, the link transmission loss results in $+0$-dBm link power. Custom-built bi-directional PM erbium doped fiber amplifier (PM-EDFA) is used in the last section of the timing link to boost the output power to $+13$ dBm. $+3$ dBm of power is reflected back by the FC partial reflector (FC-PR with 10% back reflection) and reamplified by the PM-EDFA back to $+13$ dBm. The back-propagated pulses are then combined with new laser pulses from the reference arm of FC-PBS1 in the in-loop FC-BOC. The in-loop FC-BOC measures the propagation delay change in the timing link and generates an error voltage. The error signal is processed by a PI controller and then applied to the fiber stretcher with a PZT amplifier to compensate the fast timing jitter (see Fig. 4(c)). The piezo resonance of the stretcher at 16 kHz permits a closed loop bandwidth higher than 10 kHz. The output of the PI controller is also recorded by a data acquisition card so that when it reaches its output voltage limit, the motorized-delay is activated through a computer program serving as the slow compensation to the fluctuating link delay. Finally, the output of the FC-PR and the out-of-loop reference fiber are combined in FC-PBS2 and coupled into the out-of-loop FC-BOC to evaluate the performance of the link stabilization experiment. In order to minimize the drifts coming from the length fluctuations in the FC-BOC reference paths, all setup elements are placed in a temperature-stabilized optical enclosure, except the 3.5-km fiber link spool, which is put outside and exposed to environmental fluctuations in the laboratory.

B. Results and discussion

Fig. 5 shows the measured voltage responses of the FC-BOCs against the time delay between the incoming orthogonal pulses. Due to excess coupling loss between the PM fiber and the waveguide for the reverse-generated SH, the SH power collected on the forward path is approximately 10 dB higher than that of the reverse path in FC-BOCs. Therefore, a 10-dB attenuator is inserted to symmetrize the cross-correlation curve. This issue has prevented us from reaching higher timing sensitivities for FC-BOCs when compared with bulk optics cross-correlators. Nevertheless, even with the current coupling losses, we have achieved comparable results to the previous work.[19–21] For each FC-BOC, five different measurements are performed and the mean values of the jitter-to-voltage conversion factors are 4.5 mV/fs (± 0.32 mV/fs) and 82.0 mV/fs (± 4.9 mV/fs) for the in-loop and out-of-loop FC-BOC, respectively (BPD transimpedance gain: 2×10^6 V/A, bandwidth: 150 kHz, and responsivity: 0.5 A/W).

The relative timing stability of the 3.5-km PM fiber link is continuously monitored for 200 h without interruption. The black curve in Fig. 6(a) displays the residual timing drift measured by low-pass filtering the output of out-of-loop FC-BOC at 2 Hz (without any averaging). A remaining drift of only 3.3 fs (± 0.2 fs) RMS is measured for 200 h of continuous link stabilization, and the motor delay has corrected for over 25-ps timing error. Relative temperature
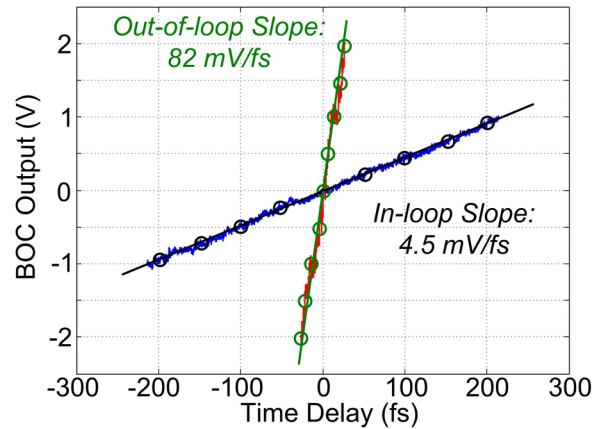
FIG. 5. Measurement results of the FC-BOC output versus the delay between the pulses. Blue curve corresponds to the in-loop and red curve corresponds to the out-of-loop FC-BOC response. Linear fits to five different measurements give average timing sensitivity of 4.5 mV/fs (±0.32 mV/fs) and 82 mV/fs (±4.9 mV/fs) for the in-loop and out-of-loop FC-BOC, respectively.

fluctuations of the 3.5-km fiber spool and the enclosure are plotted in Fig. 6(b). The maximum deviation of the temperature is about 0.18 K and 0.06 K on the case of the fiber spool and inside the enclosure, respectively. Targeted temperature stability of the tunnel in the European XFEL, biggest FEL under construction is less than 1-K change per day[28] which can be easily
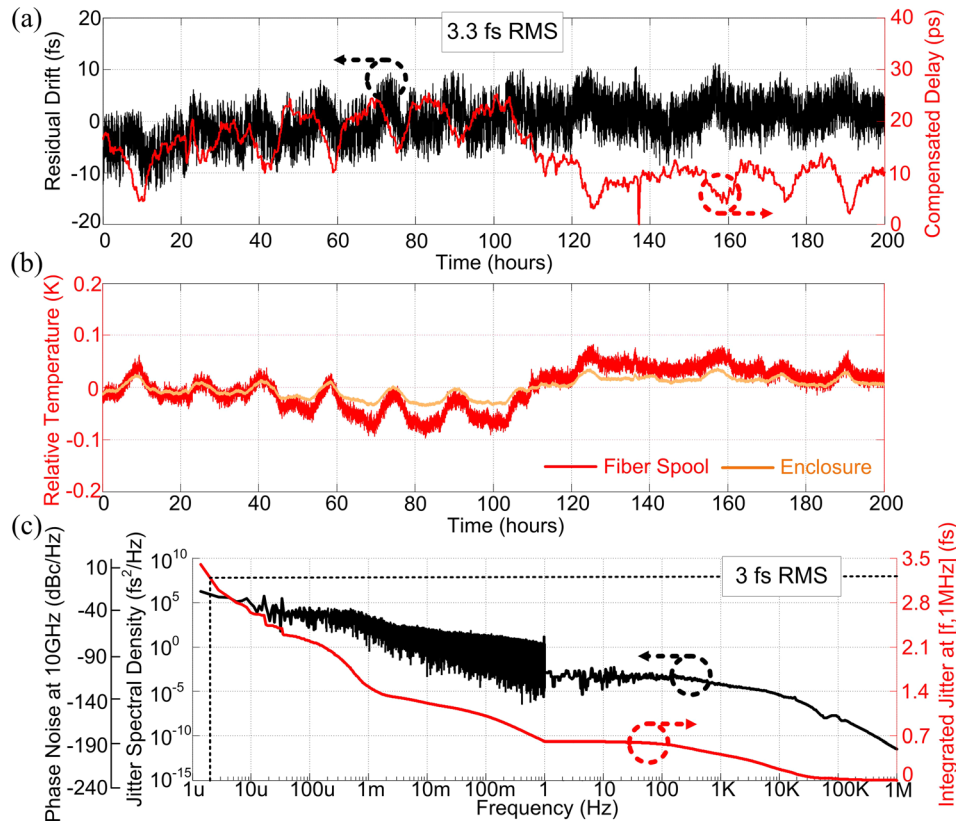

FIG. 6. Out-of-loop measurement results. (a) Black curve: timing drift for 200 h of continuous operation; red curve: corrected link propagation delay by the FC-MD. (b) Environmental conditions during the measurement, red curve: temperature measured on the 3.5-km fiber link spool; orange curve: temperature measured inside the enclosure. (c) Black curve: timing jitter spectral density and single-sideband phase noise (scaled at a 10 GHz carrier) from 1.4 μHz up to 1 MHz; red curve: its integrated jitter from frequency f up to 1 MHz.

compensated by the demonstrated setup as it can withstand ∼5.5 K average temperature fluctuation for a 3.5-km fiber link limited by the range of the FC-MD. This range can simply be extended by cascading several FC-MDs or by using other fiber-based delay elements with longer translation such as thermally tuned fiber optic delay lines.[29]

The correlation between the residual drift and the enclosure temperature (see Figs. 6(a) and 6(b)) confirms that the drift is mainly limited by the environmental fluctuations penetrating into the FC-BOCs. This is reasonable because the optical enclosure is large in volume, making it difficult to completely isolate the enclosed fibers from the laboratory environment. Even though we have spent considerable effort to splice as short fiber reference arms as possible, the system still contains in total ∼2.5 m of uncompensated fiber (reference arms of the FC-BOCs and the fiber pigtail between FC-PR and FC-PBS2). A temperature fluctuation of ∼0.1 K on 2.5-m uncompensated fiber would introduce ∼5-fs error to the timing detection due to thermal expansion and contribute directly to the final drift. Hence, the observed residual drift in our experiment agrees well with the recorded relative temperature change.

Complete jitter spectral density of the link stabilization and its integrated jitter are shown in Fig. 6(c) (black and red curves, respectively). The spectrum from 1 Hz up to 1 MHz is taken with a baseband spectrum analyzer from the out-of-loop FC-BOC; whereas, the spectrum below 1 Hz is obtained by taking the Fourier transformation of the residual drift data shown in 6(a). The total jitter above 1 Hz is kept below 0.7 fs ($\pm$0.04 fs) RMS, whereas the daily temperature fluctuations cause considerable jitter as can be seen from the frequency range below 1 mHz (red curve, Fig. 6(c)). Nevertheless, phase noise of only -20 dBc/Hz at an offset frequency of 2 μHz from a 10-GHz carrier is achieved and the total integrated jitter from 2 μHz up to 1 MHz is only 3 fs ($\pm$0.18 fs) RMS which is more than sufficient for an efficient FEL synchronization.

IV. CONCLUSION

In summary, we have successfully implemented a complete fiber-optic timing distribution system, which can be used for precise and long-term stable FEL synchronization. Jitter characterization of the master laser shows less than 170-as integrated jitter for frequencies above 10 kHz, confirming once more the excellent low-jitter properties of mode-locked lasers. We have demonstrated timing stabilization of a 3.5-km long fiber link using completely fiber-coupled elements. The out-of-loop measurement shows only 3-fs RMS link jitter integrated from 2 μHz up to 1 MHz. Long-term drift of the current setup is mainly limited by environmental fluctuations introducing timing detection errors via the uncompensated reference fiber arms. Local temperature stabilization of these reference arms would alleviate this effect and deliver better precision. This would also allow us to identify other factors playing a role in pulse propagation in fibers such as lasers inherent jitter, operational link power fluctuations, residual dispersion, and nonlinearity of the fiber link. We are currently working a numerical model to study these effects and eliminate them together with a careful experimental analysis in order to reach eventually sub-fs precision. Furthermore, the current efficiency of the FC-BOCs is limited by excess SH coupling loss but still delivers a sensitivity comparable to the bulk-optic BOCs. The next generation device will include an integrated WDM to eliminate the coupling problem, thereby increasing the performance by an order of magnitude.

Nevertheless, the current system based on FC-BOCs and PM fiber elements provides easy-to-implement, alignment-free, long-term stable, few-fs precision timing distribution under normal laboratory conditions. We believe that the demonstrated all-fiber timing distribution system can easily be deployed to an operating FEL, helping to both monitor and control electron bunch creation and pave the way for few-fs X-ray pulse generation. Such short X-ray pulses would contribute to X-ray diffraction imaging by allowing the use of much higher radiation doses in diffraction before destruction techniques.[7,30] For instance, calculations by Barty *et al.*[30] predict that one can achieve 0.3-nm resolution using 5-fs long X-ray pulses with 10^{21} W/cm^2 irradiance and 8-keV photon energy. Furthermore, the demonstrated system would allow few-fs synchronization between XFEL and external laser pulses pushing the limits of spatiotemporal resolution of XFEL pump-probe experiments. This would correspond to two orders of magnitude

improvement when compared with traditional RF phase-locking techniques used in current pump-probe setups[31] which are mainly limited by optical vs. FEL pulse jitter ($>$200 fs RMS).

[1] W. Ackermann *et al.*, "Operation of a free-electron laser from the extreme ultraviolet to the water window," Nat. Photonics **1**, 336–342 (2007).

[2] P. Emma *et al.*, "First lasing and operation of an angstrom-wavelength free-electron laser," Nat. Photonics **4**, 641–647 (2010).

[3] T. Ishikawa *et al.*, "A compact X-ray free-electron laser emitting in the sub-angstrom region," Nat. Photonics **6**, 540–544 (2012).

[4] E. Allaria *et al.*, "Highly coherent and stable pulses from the FERMI seeded free-electron laser in the extreme ultraviolet," Nat. Photonics **6**, 699–704 (2012).

[5] I. Grguras *et al.*, "Ultrafast X-ray pulse characterization at free-electron lasers," Nat. Photonics **6**(12), 852–857 (2012).

[6] J. Ulrich, A. Rudenko, and R. Moshammer, "Free-electron lasers: new avenues in molecular physics and photochemistry," Annu. Rev. Phys. Chem. **63**, 635–660 (2012).

[7] A. Barty, J. Küpper, and H. N. Chapman, "Molecular imaging using X-ray free-electron lasers," Annual Rev. Phys. Chem. **64**, 415–435 (2013).

[8] M. Altarelli *et al.*, "The European x-ray free-electron laser," Technical Design Report No. 97, DESY, 2006, pp. 1–26.

[9] A. L. Cavalieri *et al.*, "Clocking femtosecond X-rays," Phys. Rev. Lett. **94**, 114801 (2005).

[10] S. Düsterer *et al.*, "Femtosecond X-ray pulse length characterization at the Linac Coherent Light Source free-electron laser," New J. Phys. **13**, 093024 (2011).

[11] J. M. Byrd, L. Doolittle, G. Huang, J. W. Staples, R. B. Wilcox, J. Arthur, J. C. Frisch, and W. E. White, "Femtosecond synchronization of laser systems for the LCLS," in *Proceedings of IPAC2010* (2010).

[12] J. Kim, J. A. Cox, J. Chen, and F. X. Kärtner, "Drift-free femtosecond timing synchronization of remote optical and microwave sources," Nat. Photonics **2**(12), 733–736 (2008).

[13] A. J. Benedick, J. G. Fujimoto, and F. X. Kärtner, "Optical flywheels with attosecond jitter," Nat. Photonics **6**(2), 97–100 (2012).

[14] Y. Song, C. Kim, K. Jung, H. Kim, and J. Kim, "Timing jitter optimization of mode-locked Yb-fiber lasers toward the attosecond regime," Opt. Express **19**(15), 14518–14525 (2011).

[15] J. Kim, J. Chen, Z. Zhang, F. Wong, F. X. Kärtner, F. Loehl, and H. Schlarb, "Long-term femtosecond timing link stabilization using a single-crystal balanced cross correlator," Opt. Lett. **32**, 1044–1046 (2007).

[16] T. R. Schibli, J. Kim, O. Kuzucu, J. T. Gopinath, S. N. Tandon, G. S. Petrich, L. A. Kolodziejski, J. G. Fujimoto, E. P. Ippen, and F. X. Kaertner, "Attosecond active synchronization of passively mode-locked lasers by balanced cross correlation," Opt. Lett. **28**(11), 947–949 (2003).

[17] J. Kim, F. Kärtner, and F. Ludwig, "Balanced optical-microwave phase detectors for optoelectronic phase-locked loops," Opt. Lett. **31**, 3659–3661 (2006).

[18] M. Y. Peng, A. Kalaydzhyan, and F. Kärtner, "Balanced optical-microwave phase detector for sub-femtosecond optical-RF synchronization," Opt. Express **22**, 27102–27111 (2014).

[19] M. Y. Peng, P. T. Callahan, A. Nejadmalayeri, S. Valente, M. Xin, L. Grüner-Nielsen, E. Monberg, M. Yan, J. Fini, and F. Kärtner, "Long-term stable, sub-femtosecond timing distribution via a 1.2-km polarization-maintaining fiber link: Approaching 10^{-21} link stability," Opt. Express **21**, 19982–19989 (2013).

[20] K. Safak, M. Xin, M. Y. Peng, P. T. Callahan, and F. X. Kärtner, "Laser-to-laser remote transfer and synchronization with sub-fs precision over a 3.5 km fiber link," in *Proceedings of the IEEE IFCS2014* (2014), pp. 1–5.

[21] M. Xin, K. Safak, M. Y. Peng, P. T. Callahan, and F. X. Kärtner, "One-femtosecond, long-term stable remote laser synchronization over a 3.5-km fiber link," Opt. Express **22**, 14904–14912 (2014).

[22] S. Schulz *et al.*, "Femtosecond all-optical synchronization of an X-ray free-electron laser," Nat. Commun. **6**, 5938 (2015).

[23] C. Sydlo, M. K. Czwalinna, M. Felber, C. Gerth, T. Lamb, H. Schlarb, S. Schulz, F. Zummack, and S. Jablonski, "Development status of optical synchronization for the European xfel," in *Proceedings of the IBIC2013* (2013).

[24] A. H. Nejadmalayeri, F. N. C. Wong, T. D. Roberts, P. Battle, and F. X. Kärtner, "Guided wave optics in periodically poled KTP: Quadratic nonlinearity and prospects for attosecond jitter characterization," Opt. Lett. **34**(16), 2522–2524 (2009).

[25] P. T. Callahan, K. Safak, P. Battle, T. Roberts, and F. Kärtner, "Fiber-coupled balanced optical cross-correlator using PPKTP waveguides," Opt. Express **22**, 9749–9758 (2014).

[26] J. Kim, J. Chen, J. Cox, and F. Kärtner, "Attosecond-resolution timing jitter characterization of free-running mode-locked lasers," Opt. Lett. **32**, 3519–3521 (2007).

[27] F. Loehl, H. Schlarb, J. Müller, J. Kim, J. Chen, F. Wong, and F. X. Kaertner, "Sub-10 femtosecond stabilization of a fiber-link using a balanced optical cross-correlator," in *Proceedings of the IEEE PAC2007* (2007), pp. 3804–3806.

[28]W. Decking and T. Limberg, "European XFEL post-TDR description," Technical Report No. XFEL.EU TN-2013-004-01, Hamburg, 2013.

[29]B. Howley, Z. Shi, Y. Jiang, and R. T. Chen, "Thermally tuned optical fiber for true time delay generation," Opt. Laser Technol. **37**(1), 29–32 (2005).

[30]A. Barty *et al.*, "Self-terminating diffraction gates femtosecond X-ray nanocrystallography measurements," Nat. Photonics **6**, 35–40 (2012).

[31]J. M. Glownia *et al.*, "Time-resolved pump-probe experiments at the LCLS," Opt. Express **18**, 17620–17630 (2010).